Search for the $Z_1(4050)^+$ and $Z_2(4250)^+$ states in $\bar{B}^0 \to \chi_{c1} K^- \pi^+$ and $B^+ \to \chi_{c1} K_S^0 \pi^+$

J. P. Lees,[1] V. Poireau,[1] V. Tisserand,[1] J. Garra Tico,[2] E. Grauges,[2] M. Martinelli,[3a,3b] D. A. Milanes,[3a] A. Palano,[3a,3b] M. Pappagallo,[3a,3b] G. Eigen,[4] B. Stugu,[4] D. N. Brown,[5] L. T. Kerth,[5] Yu. G. Kolomensky,[5] G. Lynch,[5] H. Koch,[6] T. Schroeder,[6] D. J. Asgeirsson,[7] C. Hearty,[7] T. S. Mattison,[7] J. A. McKenna,[7] A. Khan,[8] V. E. Blinov,[9] A. R. Buzykaev,[9] V. P. Druzhinin,[9] V. B. Golubev,[9] E. A. Kravchenko,[9] A. P. Onuchin,[9] S. I. Serednyakov,[9] Yu. I. Skovpen,[9] E. P. Solodov,[9] K. Yu. Todyshev,[9] A. N. Yushkov,[9] M. Bondioli,[10] D. Kirkby,[10] A. J. Lankford,[10] M. Mandelkern,[10] D. P. Stoker,[10] H. Atmacan,[11] J. W. Gary,[11] F. Liu,[11] O. Long,[11] G. M. Vitug,[11] C. Campagnari,[12] T. M. Hong,[12] D. Kovalskyi,[12] J. D. Richman,[12] C. A. West,[12] A. M. Eisner,[13] J. Kroseberg,[13] W. S. Lockman,[13] A. J. Martinez,[13] T. Schalk,[13] B. A. Schumm,[13] A. Seiden,[13] C. H. Cheng,[14] D. A. Doll,[14] B. Echenard,[14] K. T. Flood,[14] D. G. Hitlin,[14] P. Ongmongkolkul,[14] F. C. Porter,[14] A. Y. Rakitin,[14] R. Andreassen,[15] Z. Huard,[15] B. T. Meadows,[15] M. D. Sokoloff,[15] L. Sun,[15] P. C. Bloom,[16] W. T. Ford,[16] A. Gaz,[16] M. Nagel,[16] U. Nauenberg,[16] J. G. Smith,[16] S. R. Wagner,[16] R. Ayad,[17,*] W. H. Toki,[17] B. Spaan,[18] M. J. Kobel,[19] K. R. Schubert,[19] R. Schwierz,[19] D. Bernard,[20] M. Verderi,[20] P. J. Clark,[21] S. Playfer,[21] D. Bettoni,[22a] C. Bozzi,[22b] R. Calabrese,[22a,22b] G. Cibinetto,[22a,22b] E. Fioravanti,[22a,22b] I. Garzia,[22a,22b] E. Luppi,[22a,22b] M. Munerato,[22a,22b] M. Negrini,[22a,22b] L. Piemontese,[22a] V. Santoro,[22a] R. Baldini-Ferroli,[23] A. Calcaterra,[23] R. de Sangro,[23] G. Finocchiaro,[23] M. Nicolaci,[23] P. Patteri,[23] I. M. Peruzzi,[23,†] M. Piccolo,[23] M. Rama,[23] A. Zallo,[23] R. Contri,[24a,24b] E. Guido,[24a,24b] M. Lo Vetere,[24a,24b] M. R. Monge,[24a,24b] S. Passaggio,[24a] C. Patrignani,[24a,24b] E. Robutti,[24a] B. Bhuyan,[25] V. Prasad,[25] C. L. Lee,[26] M. Morii,[26] A. J. Edwards,[27] A. Adametz,[28] J. Marks,[28] U. Uwer,[28] F. U. Bernlochner,[29] H. M. Lacker,[29] T. Lueck,[29] P. D. Dauncey,[30] P. K. Behera,[31] U. Mallik,[31] C. Chen,[32] J. Cochran,[32] W. T. Meyer,[32] S. Prell,[32] E. I. Rosenberg,[32] A. E. Rubin,[32] A. V. Gritsan,[33] Z. J. Guo,[33] N. Arnaud,[34] M. Davier,[34] D. Derkach,[34] G. Grosdidier,[34] F. Le Diberder,[34] A. M. Lutz,[34] B. Malaescu,[34] P. Roudeau,[34] M. H. Schune,[34] A. Stocchi,[34] G. Wormser,[34] D. J. Lange,[35] D. M. Wright,[35] I. Bingham,[36] C. A. Chavez,[36] J. P. Coleman,[36] J. R. Fry,[36] E. Gabathuler,[36] D. E. Hutchcroft,[36] D. J. Payne,[36] C. Touramanis,[36] A. J. Bevan,[37] F. Di Lodovico,[37] R. Sacco,[37] M. Sigamani,[37] G. Cowan,[38] D. N. Brown,[39] C. L. Davis,[39] A. G. Denig,[40] M. Fritsch,[40] W. Gradl,[40] A. Hafner,[40] E. Prencipe,[40] K. E. Alwyn,[41] D. Bailey,[41] R. J. Barlow,[41,‡] G. Jackson,[41] G. D. Lafferty,[41] E. Behn,[42] R. Cenci,[42] B. Hamilton,[42] A. Jawahery,[42] D. A. Roberts,[42] G. Simi,[42] C. Dallapiccola,[43] R. Cowan,[44] D. Dujmic,[44] G. Sciolla,[44] D. Lindemann,[45] P. M. Patel,[45] S. H. Robertson,[45] M. Schram,[45] P. Biassoni,[46a,46b] N. Neri,[46a,46b] F. Palombo,[46a,46b] S. Stracka,[46a,46b] L. Cremaldi,[47] R. Godang,[47,§] R. Kroeger,[47] P. Sonnek,[47] D. J. Summers,[47] X. Nguyen,[48] M. Simard,[48] P. Taras,[48] G. De Nardo,[49a,49b] D. Monorchio,[49a,49b] G. Onorato,[49a,49b] C. Sciacca,[49a,49b] G. Raven,[50] H. L. Snoek,[50] C. P. Jessop,[51] K. J. Knoepfel,[51] J. M. LoSecco,[51] W. F. Wang,[51] K. Honscheid,[52] R. Kass,[52] J. Brau,[53] R. Frey,[53] N. B. Sinev,[53] D. Strom,[53] E. Torrence,[53] E. Feltresi,[54a,54b] N. Gagliardi,[54a,54b] M. Margoni,[54a,54b] M. Morandin,[54a] M. Posocco,[54a] M. Rotondo,[54a] F. Simonetto,[54a,54b] R. Stroili,[54a,54b] S. Akar,[55] E. Ben-Haim,[55] M. Bomben,[55] G. R. Bonneaud,[55] H. Briand,[55] G. Calderini,[55] J. Chauveau,[55] O. Hamon,[55] Ph. Leruste,[55] G. Marchiori,[55] J. Ocariz,[55] S. Sitt,[55] M. Biasini,[56a,56b] E. Manoni,[56a,56b] S. Pacetti,[56a,56b] A. Rossi,[56a,56b] C. Angelini,[57a,57b] G. Batignani,[57a,57b] S. Bettarini,[57a,57b] M. Carpinelli,[57a,57b,‖] G. Casarosa,[57a,57b] A. Cervelli,[57a,57b] F. Forti,[57a,57b] M. A. Giorgi,[57a,57b] A. Lusiani,[57a,57c] B. Oberhof,[57a,57b] E. Paoloni,[57a,57b] A. Perez,[57a] G. Rizzo,[57a,57b] J. J. Walsh,[57a] D. Lopes Pegna,[58] C. Lu,[58] J. Olsen,[58] A. J. S. Smith,[58] A. V. Telnov,[58] F. Anulli,[59a] G. Cavoto,[59a] R. Faccini,[59a,59b] F. Ferrarotto,[59a] F. Ferroni,[59a,59b] M. Gaspero,[59a,59b] L. Li Gioi,[59a] M. A. Mazzoni,[59a] G. Piredda,[59a] C. Bünger,[60] O. Grünberg,[60] T. Hartmann,[60] T. Leddig,[60] H. Schröder,[60] C. Voss,[60] R. Waldi,[60] T. Adye,[61] E. O. Olaiya,[61] F. F. Wilson,[61] S. Emery,[62] G. Hamel de Monchenault,[62] G. Vasseur,[62] Ch. Yèche,[62] D. Aston,[63] D. J. Bard,[63] R. Bartoldus,[63] C. Cartaro,[63] M. R. Convery,[63] J. Dorfan,[63] G. P. Dubois-Felsmann,[63] W. Dunwoodie,[63] M. Ebert,[63] R. C. Field,[63] M. Franco Sevilla,[63] B. G. Fulsom,[63] A. M. Gabareen,[63] M. T. Graham,[63] P. Grenier,[63] C. Hast,[63] W. R. Innes,[63] M. H. Kelsey,[63] P. Kim,[63] M. L. Kocian,[63] D. W. G. S. Leith,[63] P. Lewis,[63] B. Lindquist,[63] S. Luitz,[63] V. Luth,[63] H. L. Lynch,[63] D. B. MacFarlane,[63] D. R. Muller,[63] H. Neal,[63] S. Nelson,[63] M. Perl,[63] T. Pulliam,[63] B. N. Ratcliff,[63] A. Roodman,[63] A. A. Salnikov,[63] R. H. Schindler,[63] A. Snyder,[63] D. Su,[63] M. K. Sullivan,[63] J. Va'vra,[63] A. P. Wagner,[63] M. Weaver,[63] W. J. Wisniewski,[63] M. Wittgen,[63] D. H. Wright,[63] H. W. Wulsin,[63] A. K. Yarritu,[63] C. C. Young,[63] V. Ziegler,[63] W. Park,[64] M. V. Purohit,[64] R. M. White,[64] J. R. Wilson,[64] A. Randle-Conde,[65] S. J. Sekula,[65] M. Bellis,[66] J. F. Benitez,[66] P. R. Burchat,[66] T. S. Miyashita,[66] M. S. Alam,[67] J. A. Ernst,[67] R. Gorodeisky,[68] N. Guttman,[68] D. R. Peimer,[68] A. Soffer,[68] P. Lund,[69] S. M. Spanier,[69] R. Eckmann,[70] J. L. Ritchie,[70] A. M. Ruland,[70] C. J. Schilling,[70] R. F. Schwitters,[70] B. C. Wray,[70] J. M. Izen,[71] X. C. Lou,[71] F. Bianchi,[72a,72b] D. Gamba,[72a,72b] L. Lanceri,[73a,73b] L. Vitale,[73a,73b] F. Martinez-Vidal,[74] A. Oyanguren,[74] H. Ahmed,[75] J. Albert,[75] Sw. Banerjee,[75] H. H. F. Choi,[75] G. J. King,[75] R. Kowalewski,[75]

M. J. Lewczuk,[75] I. M. Nugent,[75] J. M. Roney,[75] R. J. Sobie,[75] N. Tasneem,[75] T. J. Gershon,[76] P. F. Harrison,[76] T. E. Latham,[76] E. M. T. Puccio,[76] H. R. Band,[77] S. Dasu,[77] Y. Pan,[77] R. Prepost,[77] and S. L. Wu[77]

(*BABAR* Collaboration)

[1]*Laboratoire d'Annecy-le-Vieux de Physique des Particules (LAPP), Université de Savoie, CNRS/IN2P3, F-74941 Annecy-Le-Vieux, France*
[2]*Universitat de Barcelona, Facultat de Fisica, Departament ECM, E-08028 Barcelona, Spain*
[3a]*INFN Sezione di Bari, I-70126 Bari, Italy*
[3b]*Dipartimento di Fisica, Università di Bari, I-70126 Bari, Italy*
[4]*University of Bergen, Institute of Physics, N-5007 Bergen, Norway*
[5]*Lawrence Berkeley National Laboratory and University of California, Berkeley, California 94720, USA*
[6]*Ruhr Universität Bochum, Institut für Experimentalphysik 1, D-44780 Bochum, Germany*
[7]*University of British Columbia, Vancouver, British Columbia, Canada V6T 1Z1*
[8]*Brunel University, Uxbridge, Middlesex UB8 3PH, United Kingdom*
[9]*Budker Institute of Nuclear Physics, Novosibirsk 630090, Russia*
[10]*University of California at Irvine, Irvine, California 92697, USA*
[11]*University of California at Riverside, Riverside, California 92521, USA*
[12]*University of California at Santa Barbara, Santa Barbara, California 93106, USA*
[13]*University of California at Santa Cruz, Institute for Particle Physics, Santa Cruz, California 95064, USA*
[14]*California Institute of Technology, Pasadena, California 91125, USA*
[15]*University of Cincinnati, Cincinnati, Ohio 45221, USA*
[16]*University of Colorado, Boulder, Colorado 80309, USA*
[17]*Colorado State University, Fort Collins, Colorado 80523, USA*
[18]*Technische Universität Dortmund, Fakultät Physik, D-44221 Dortmund, Germany*
[19]*Technische Universität Dresden, Institut für Kern- und Teilchenphysik, D-01062 Dresden, Germany*
[20]*Laboratoire Leprince-Ringuet, Ecole Polytechnique, CNRS/IN2P3, F-91128 Palaiseau, France*
[21]*University of Edinburgh, Edinburgh EH9 3JZ, United Kingdom*
[22a]*INFN Sezione di Ferrara, I-44100 Ferrara, Italy*
[22b]*Dipartimento di Fisica, Università di Ferrara, I-44100 Ferrara, Italy*
[23]*INFN Laboratori Nazionali di Frascati, I-00044 Frascati, Italy*
[24a]*INFN Sezione di Genova, Italy*
[24b]*Dipartimento di Fisica, Università di Genova, I-16146 Genova, Italy*
[25]*Indian Institute of Technology Guwahati, Guwahati, Assam, 781 039, India*
[26]*Harvard University, Cambridge, Massachusetts 02138, USA*
[27]*Harvey Mudd College, Claremont, California 91711*
[28]*Universität Heidelberg, Physikalisches Institut, Philosophenweg 12, D-69120 Heidelberg, Germany*
[29]*Humboldt-Universität zu Berlin, Institut für Physik, Newtonstraße 15, D-12489 Berlin, Germany*
[30]*Imperial College London, London, SW7 2AZ, United Kingdom*
[31]*University of Iowa, Iowa City, Iowa 52242, USA*
[32]*Iowa State University, Ames, Iowa 50011-3160, USA*
[33]*Johns Hopkins University, Baltimore, Maryland 21218, USA*
[34]*Laboratoire de l'Accélérateur Linéaire, IN2P3/CNRS et Université Paris-Sud 11, Centre Scientifique d'Orsay, B.P. 34, F-91898 Orsay Cedex, France*
[35]*Lawrence Livermore National Laboratory, Livermore, California 94550, USA*
[36]*University of Liverpool, Liverpool L69 7ZE, United Kingdom*
[37]*Queen Mary, University of London, London, E1 4NS, United Kingdom*
[38]*University of London, Royal Holloway and Bedford New College, Egham, Surrey TW20 0EX, United Kingdom*
[39]*University of Louisville, Louisville, Kentucky 40292, USA*
[40]*Johannes Gutenberg-Universität Mainz, Institut für Kernphysik, D-55099 Mainz, Germany*
[41]*University of Manchester, Manchester M13 9PL, United Kingdom*
[42]*University of Maryland, College Park, Maryland 20742, USA*
[43]*University of Massachusetts, Amherst, Massachusetts 01003, USA*
[44]*Massachusetts Institute of Technology, Laboratory for Nuclear Science, Cambridge, Massachusetts 02139, USA*
[45]*McGill University, Montréal, Québec, Canada H3A 2T8*
[46a]*INFN Sezione di Milano, Italy*
[46b]*Dipartimento di Fisica, Università di Milano, I-20133 Milano, Italy*
[47]*University of Mississippi, University, Mississippi 38677, USA*
[48]*Université de Montréal, Physique des Particules, Montréal, Québec, Canada H3C 3J7*
[49a]*INFN Sezione di Napoli, I-80126 Napoli, Italy*

[49b]Dipartimento di Scienze Fisiche, Università di Napoli Federico II, I-80126 Napoli, Italy
[50]NIKHEF, National Institute for Nuclear Physics and High Energy Physics, NL-1009 DB Amsterdam, The Netherlands
[51]University of Notre Dame, Notre Dame, Indiana 46556, USA
[52]Ohio State University, Columbus, Ohio 43210, USA
[53]University of Oregon, Eugene, Oregon 97403, USA
[54a]INFN Sezione di Padova, I-35131 Padova, Italy
[54b]Dipartimento di Fisica, Università di Padova, I-35131 Padova, Italy
[55]Laboratoire de Physique Nucléaire et de Hautes Energies, IN2P3/CNRS, Université Pierre et Marie Curie-Paris6, Université Denis Diderot-Paris7, F-75252 Paris, France
[56a]INFN Sezione di Perugia, I-06100 Perugia, Italy
[56b]Dipartimento di Fisica, Università di Perugia, I-06100 Perugia, Italy
[57a]INFN Sezione di Pisa, I-56127 Pisa, Italy
[57b]Dipartimento di Fisica, Università di Pisa; Scuola Normale Superiore di Pisa, I-56127 Pisa, Italy
[57c]Scuola Normale Superiore di Pisa, I-56127 Pisa, Italy
[58]Princeton University, Princeton, New Jersey 08544, USA
[59a]INFN Sezione di Roma, I-00185 Roma, Italy
[59b]Dipartimento di Fisica, Università di Roma La Sapienza, I-00185 Roma, Italy
[60]Universität Rostock, D-18051 Rostock, Germany
[61]Rutherford Appleton Laboratory, Chilton, Didcot, Oxon, OX11 0QX, United Kingdom
[62]CEA, Irfu, SPP, Centre de Saclay, F-91191 Gif-sur-Yvette, France
[63]SLAC National Accelerator Laboratory, Stanford, California 94309, USA
[64]University of South Carolina, Columbia, South Carolina 29208, USA
[65]Southern Methodist University, Dallas, Texas 75275, USA
[66]Stanford University, Stanford, California 94305-4060, USA
[67]State University of New York, Albany, New York 12222, USA
[68]Tel Aviv University, School of Physics and Astronomy, Tel Aviv, 69978, Israel
[69]University of Tennessee, Knoxville, Tennessee 37996, USA
[70]University of Texas at Austin, Austin, Texas 78712, USA
[71]University of Texas at Dallas, Richardson, Texas 75083, USA
[72a]INFN Sezione di Torino, I-10125 Torino, Italy
[72b]Dipartimento di Fisica Sperimentale, Università di Torino, I-10125 Torino, Italy
[73a]INFN Sezione di Trieste, I-34127 Trieste, Italy
[73b]Dipartimento di Fisica, Università di Trieste, I-34127 Trieste, Italy
[74]IFIC, Universitat de Valencia-CSIC, E-46071 Valencia, Spain
[75]University of Victoria, Victoria, British Columbia, Canada V8W 3P6
[76]Department of Physics, University of Warwick, Coventry CV4 7AL, United Kingdom
[77]University of Wisconsin, Madison, Wisconsin 53706, USA

(Received 25 November 2011; published 16 March 2012)

We search for the $Z_1(4050)^+$ and $Z_2(4250)^+$ states, reported by the Belle Collaboration, decaying to $\chi_{c1}\pi^+$ in the decays $\bar{B}^0 \to \chi_{c1}K^-\pi^+$ and $B^+ \to \chi_{c1}K^0_S\pi^+$ where $\chi_{c1} \to J/\psi\gamma$. The data were collected with the *BABAR* detector at the SLAC PEP-II asymmetric-energy e^+e^- collider operating at center-of-mass energy 10.58 GeV, and correspond to an integrated luminosity of 429 fb^{-1}. In this analysis, we model the background-subtracted, efficiency-corrected $\chi_{c1}\pi^+$ mass distribution using the $K\pi$ mass distribution and the corresponding normalized $K\pi$ Legendre-polynomial moments, and then test the need for the inclusion of resonant structures in the description of the $\chi_{c1}\pi^+$ mass distribution. No evidence is found for the $Z_1(4050)^+$ and $Z_2(4250)^+$ resonances, and 90% confidence level upper limits on the branching fractions are reported for the corresponding B-meson decay modes.

DOI: 10.1103/PhysRevD.85.052003 PACS numbers: 12.39.Mk, 12.40.Yx, 13.25.Hw, 14.40.Rt

I. INTRODUCTION

The Belle Collaboration has reported the observation of two resonancelike structures in the study of $\bar{B}^0 \to \chi_{c1}K^-\pi^+$ [1]. These are labeled as $Z_1(4050)^+$ and $Z_2(4250)^+$, both decaying to $\chi_{c1}\pi^+$ [2]. The Belle Collaboration also reported the observation of a resonancelike structure, $Z(4430)^+ \to \psi(2S)\pi^+$, in the analysis of $B \to \psi(2S)K\pi$ [3,4]. These claims have generated a great

*Now at Temple University, Philadelphia, PA 19122, USA.
†Also with Università di Perugia, Dipartimento di Fisica, Perugia, Italy.
‡Now at the University of Huddersfield, Huddersfield HD1 3DH, UK.
§Now at University of South Alabama, Mobile, AL 36688, USA.
‖Also with Università di Sassari, Sassari, Italy.

deal of interest [5]. Such states must have a minimum quark content $c\bar{c}\,\bar{d}\,u$, and thus would represent an unequivocal manifestation of four-quark meson states.

The *BABAR* Collaboration did not see the $Z(4430)^+$ in an analysis of the decay $B \to \psi(2S)K\pi$ [6]. Points of discussion are as follows:

(i) The method of making slices of a three-body B decay Dalitz plot can produce peaks which may be due to interference effects, not resonances.

(ii) The angular structure of the $B \to \psi(2S)K\pi$ decay is rather complex and cannot be described adequately by only the two variables used in a simple Dalitz plot analysis.

In the *BABAR* analysis [6], the $B \to J/\psi K\pi$ decay does not show evidence for resonances either in the $J/\psi\pi$ or in the $J/\psi K$ systems. All resonance activity seems confined to the $K\pi$ system. It is also observed that the angular distributions, expressed in terms of the $K\pi$ Legendre-polynomial moments, show strong similarities between $B \to \psi(2S)K\pi$ and $B \to J/\psi K\pi$ decays. Therefore, the angular information provided by the $B \to J/\psi K\pi$ decay can be used to describe the $B \to \psi(2S)K\pi$ decay. It is also observed that a localized structure in the $\psi(2S)\pi$ mass spectrum would yield high angular momentum Legendre-polynomial moments in the $K\pi$ system. Therefore, a good description of the $\psi(2S)\pi$ data using only $K\pi$ moments up to $L = 5$ also suggests the absence of narrow resonant structure in the $\psi(2S)\pi$ system.

In this paper, we examine $B \to \chi_{c1}K\pi$ decays following an analysis procedure similar to that used in Ref. [6]. In contrast to the analysis of Ref. [1], we model the background-subtracted, efficiency-corrected $\chi_{c1}\pi^+$ mass distribution using the $K\pi$ mass distribution and the corresponding normalized $K\pi$ Legendre-polynomial moments, and then test the need for the inclusion of resonant structures in the description of the $\chi_{c1}\pi^+$ mass distribution.

This paper is organized as follows. A short description of the *BABAR* experiment is given in Sec. II, and the data selection is described in Sec. III. Section IV shows the data, while Secs. V and VI are devoted to the calculation of the efficiency and the extraction of branching fraction values, respectively. In Sec. VII we describe the fits to the $K\pi$ mass spectra, and in Sec. VIII we show the Legendre-polynomial moments. In Sec. IX we report the description of the $\chi_{c1}\pi^+$ mass spectra, while Sec. X is devoted to the calculation of limits on the production of the $Z_1(4050)^+$ and $Z_2(4250)^+$ resonances. We summarize our results in Sec. XI.

II. THE *BABAR* EXPERIMENT

This analysis is based on a data sample of 429 fb^{-1} recorded at the $\Upsilon(4S)$ resonance by the *BABAR* detector at the PEP-II asymmetric-energy e^+e^- storage rings. The *BABAR* detector is described in detail elsewhere [7]. Charged particles are detected and their momenta measured with a combination of a cylindrical drift chamber and a silicon vertex tracker, both operating within the 1.5 T magnetic field of a superconducting solenoid. Information from a ring-imaging Cherenkov detector is combined with specific ionization measurements from the silicon vertex tracker and cylindrical drift chamber to identify charged kaon and pion candidates. Photon energy and position are measured with a CsI(Tl) electromagnetic calorimeter, which is also used to identify electrons. The return yoke of the superconducting coil is instrumented with resistive plate chambers for the identification of muons. For the later part of the experiment the barrel-region chambers were replaced by limited streamer tubes [8].

III. DATA SELECTION

We reconstruct events in the decay modes [9]:

$$\bar{B}^0 \to \chi_{c1}K^-\pi^+, \tag{1}$$

$$B^+ \to \chi_{c1}K_S^0\pi^+, \tag{2}$$

where $\chi_{c1} \to J/\psi\gamma$, and $J/\psi \to \mu^+\mu^-$ or $J/\psi \to e^+e^-$.

For each candidate, we first reconstruct the J/ψ by geometrically constraining an identified e^+e^- or $\mu^+\mu^-$ pair of tracks to a common vertex point and requiring a χ^2 fit probability greater than 0.1%. For $J/\psi \to e^+e^-$ we introduce bremsstrahlung energy-loss recovery. If an electron-associated photon cluster is found in the electromagnetic calorimeter, its three-momentum vector is incorporated into the calculation of $m(e^+e^-)$ [10]. The fit to the J/ψ candidates includes the constraint to the nominal J/ψ mass value [2].

A K_S^0 candidate is formed by geometrically constraining a pair of oppositely charged tracks to a common vertex (χ^2 fit probability greater than 0.1%). For the two tracks the pion mass is assumed without particle-identification requirements. The K_S^0 fit includes the constraint to the nominal mass value.

The J/ψ, $K^\pm$, and $\pi^\pm$ candidates forming a B meson decay candidate are geometrically constrained to a common vertex, and a χ^2 fit probability greater than 0.1% is required. Particle identification is applied to both K and π candidates. The K_S^0 flight length with respect to the B^+ vertex must be greater than 0.2 cm.

A study of the scatter diagram E_γ vs $m(J/\psi\gamma)$ (not shown) reveals that no χ_{c1} signal is kinematically possible for $E_\gamma < 190$ MeV. Therefore, we consider only photons with a laboratory energy above this value. We select the χ_{c1} signal within $\pm 2\sigma_{\chi_{c1}}$ of the χ_{c1} mass, where $\sigma_{\chi_{c1}}$ and the χ_{c1} mass are obtained from fits to the $J/\psi\gamma$ mass spectra using a Gaussian function for the signal and a second-order polynomial for the background, separated by B and J/ψ decay modes. The values of $\sigma_{\chi_{c1}}$ range from 14.6 MeV/c^2 to 17.6 MeV/c^2.

TABLE I. Resolution parameter values from fits to the ΔE and $m_{\rm ES}$ distributions.

Channel	$\sigma_{\Delta E}$(MeV)	$\sigma_{m_{\rm ES}}$(MeV/c^2)	Events	Purity %
$\bar{B}^0 \to \chi_{c1} K^- \pi^+$ $(\mu^+\mu^-)$	6.96 ± 0.34	2.60 ± 0.10	980	79.3 ± 1.3
$\bar{B}^0 \to \chi_{c1} K^- \pi^+$ (e^+e^-)	7.81 ± 0.43	2.77 ± 0.12	883	77.1 ± 1.4
$B^+ \to \chi_{c1} K^0_S \pi^+$ $(\mu^+\mu^-)$	6.65 ± 0.55	2.65 ± 0.27	299	81.7 ± 2.2
$B^+ \to \chi_{c1} K^0_S \pi^+$ (e^+e^-)	7.52 ± 0.70	2.65 ± 0.18	329	77.5 ± 2.3

We further define B meson decay candidates using the energy difference $\Delta E \equiv E^*_B - \sqrt{s}/2$ in the center-of-mass (c.m.) frame and the beam-energy-substituted mass defined as $m_{\rm ES} \equiv \sqrt{((s/2 + \vec{p}_i \cdot \vec{p}_B)/E_i)^2 - \vec{p}^{\,2}_B}$, where $(E_i, \vec{p}_i)$ is the initial state e^+e^- four-momentum vector in the laboratory frame and $\sqrt{s}$ is the c.m. energy. In the above expressions E^*_B is the B meson candidate energy in the c.m. frame, and $\vec{p}_B$ is its laboratory frame momentum. The B decay signal events are selected within $\pm 2.0\sigma_{m_{\rm ES}}$ of the fitted central value, where the $\sigma_{m_{\rm ES}}$ values are listed in Table I and are determined by fits of a Gaussian function plus an ARGUS function [11] to the data.

The resulting ΔE distributions have been fitted with a linear background function and a signal Gaussian function whose width values ($\sigma_{\Delta \rm E}$) are also listed in Table I. Further background rejection is performed by selecting events within $\pm 2.0\sigma_{\Delta E}$ of zero. Table I also gives the values of event yield and purity, where the *purity* is defined as signal/(signal + background). The ΔE distributions shown in Fig. 1 have been summed over the $J/\psi \to \mu^+\mu^-$ and $J/\psi \to e^+e^-$ decay modes. Clear signals of the B decay modes (1) and (2) can be seen. We obtain 1863 candidates for $\bar{B}^0 \to \chi_{c1} K^- \pi^+$ decays with 78% purity, and 628 $B^+ \to \chi_{c1} K^0_S \pi^+$ events with 79% purity. A study of the ΔE and $J/\psi\gamma$ spectra in the sideband regions does not show any B or χ_{c1} signal, respectively. We conclude that the observed background is consistent with being entirely of combinatorial origin.

The resulting $J/\psi\gamma$ invariant mass distributions for channels (1) and (2) are shown in Fig. 2.

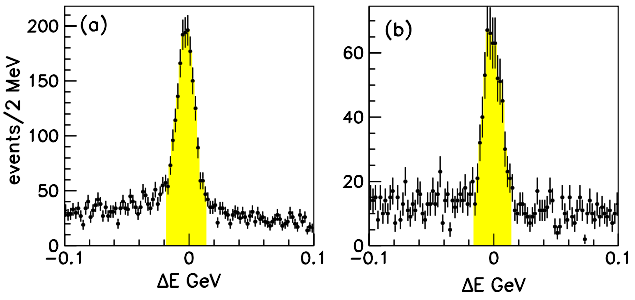

FIG. 1 (color online). Distributions of ΔE for (a) $\bar{B}^0 \to \chi_{c1} K^- \pi^+$ and (b) $B^+ \to \chi_{c1} K^0_S \pi^+$ summed over the J/ψ decay modes; the χ_{c1} and $m_{\rm ES}$ selection criteria have been applied. The shaded areas indicate the signal regions.

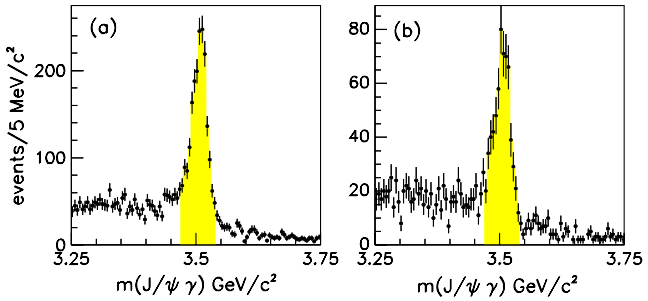

FIG. 2 (color online). The $J/\psi\gamma$ mass distribution for (a) $\bar{B}^0 \to \chi_{c1} K^- \pi^+$ and (b) $B^+ \to \chi_{c1} K^0_S \pi^+$ candidates, summed over the J/ψ decay modes. The $m_{\rm ES}$ and ΔE selection criteria have been applied. The shaded areas indicate the signal regions.

In order to estimate the background contribution in the signal region, we define ΔE sideband regions in the intervals $(7\text{–}9)\sigma_{\Delta E}$ on both sides of zero. We obtain a "-background-subtracted" distribution of events by subtracting the corresponding distribution for ΔE sideband events from that of events in the signal region.

IV. DALITZ PLOTS

The Dalitz plots for $\bar{B}^0 \to \chi_{c1} K^- \pi^+$ events in the signal and sideband regions are shown in Fig. 3. The shaded area defines the Dalitz plot boundary; it is obtained from a simple phase-space Monte Carlo (MC) simulation [12] of B decays, smeared by the experimental resolution. For the sidebands, events can lie outside the boundary. We observe a vertical band due to the presence of the

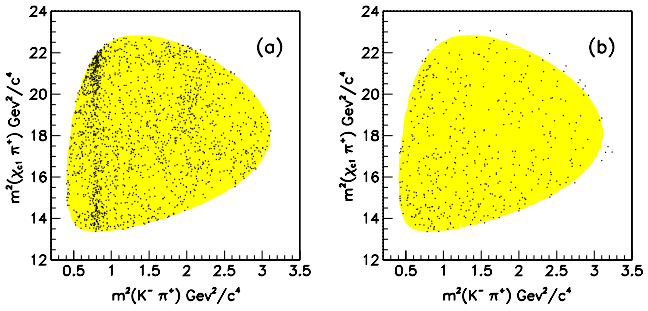

FIG. 3 (color online). Dalitz plot for $\bar{B}^0 \to \chi_{c1} K^- \pi^+$ in (a) the signal region and (b) the ΔE sidebands. The shaded area defines the Dalitz plot boundary.

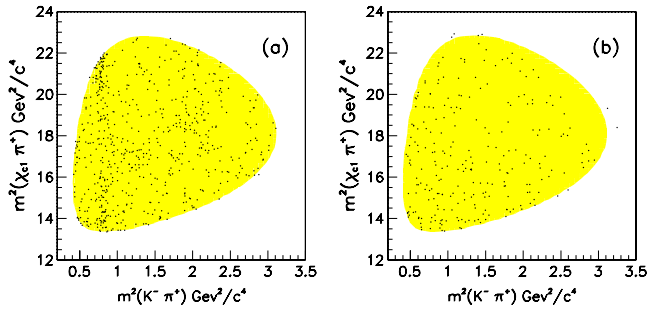

FIG. 4 (color online). Dalitz plot for $B^+ \to \chi_{c1}K^0_S\pi^+$ in (a) the signal region and (b) the ΔE sidebands. The shaded area defines the Dalitz plot boundary.

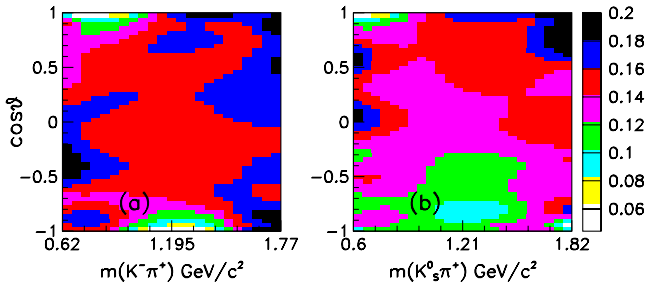

FIG. 5 (color online). Fitted efficiency on the $\cos\theta$ vs. $m(K\pi)$ plane for (a) $\bar{B}^0 \to \chi_{c1}K^-\pi^+$ and (b) $B^+ \to \chi_{c1}K^0_S\pi^+$ summed over the J/ψ decay modes.

$\bar{K}^*(892)^0$ resonance and a weaker band due to the $\bar{K}^*_2(1430)^0$ resonance. We do not observe significant accumulation of events in any horizontal band.

The Dalitz plots for $B^+ \to \chi_{c1}K^0_S\pi^+$ candidates in the signal and sideband regions are shown in Fig. 4 and show features similar to those in Fig. 3.

V. EFFICIENCY

To compute the efficiency, signal MC events (full-MC) for the different channels have been generated using a detailed detector simulation where B mesons decay uniformly in phase space. They are reconstructed and analyzed in the same way as real events. We express the efficiency as a function of $m(K\pi)$ and $\cos\theta$, the normalized dot product between the χ_{c1} momentum and that of the kaon momentum, both in the $K\pi$ rest frame. To smooth statistical fluctuations, this efficiency is then parametrized as follows.

We first fit the efficiency as a function of $\cos\theta$ in separate 50 MeV$/c^2$ intervals of $m(K\pi)$, in terms of Legendre polynomials up to $L = 12$:

$$\epsilon(\cos\theta) = \sum_{L=0}^{12} a_L(m)Y^0_L(\cos\theta). \quad (3)$$

For each value of L, we fit the $a_L(m)$ as a function of $m(K\pi)$ using a sixth-order polynomial in $m(K\pi)$. The resulting fitted efficiency for $\bar{B}^0$ decay is shown in Fig. 5(a). We observe a significant decrease in efficiency for $\cos\theta \sim +1$ and $0.72 < m(K^-\pi^+) < 0.92$ GeV$/c^2$, and for $\cos\theta \sim -1$ and $0.97 < m(K^-\pi^+) < 1.27$ GeV$/c^2$. The former is due to the failure to reconstruct pions with low momentum in the laboratory frame and the latter to a similar failure for kaons. A similar effect is observed in Fig. 5(b) for the B^+ decay mode.

In Fig. 6 we plot the efficiency projection as a function of $m(\chi_{c1}\pi^+)$ for channels (1) and (2), summed over the J/ψ decay modes. We observe a loss in efficiency at the edges of the $\chi_{c1}\pi^+$ mass range. However, these losses do not affect the regions of the reported Z resonances. Using these fitted functions we obtain efficiency-corrected

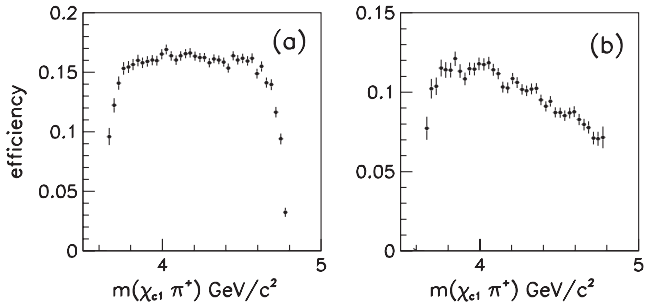

FIG. 6. Efficiency as a function of $m(\chi_{c1}\pi^+)$ for (a) $\bar{B}^0 \to \chi_{c1}K^-\pi^+$ and (b) $B^+ \to \chi_{c1}K^0_S\pi^+$ summed over the J/ψ decay modes.

distributions by weighting each event by the inverse of the efficiency at its $(m(K\pi), \cos\theta)$ location.

VI. BRANCHING FRACTIONS

We measure the branching fractions for $\bar{B}^0 \to \chi_{c1}K^-\pi^+$ and $B^+ \to \chi_{c1}K^0_S\pi^+$ relative to $B^0 \to J/\psi K^+\pi^-$ and $B^+ \to J/\psi K^0_S\pi^+$, respectively. In this way several systematic uncertainties (namely, uncertainties on the number of $B\bar{B}$ mesons, particle identification, tracking efficiency, data-MC differences, secondary branching fractions) cancel.

To obtain the yields, for each B decay mode we perform new fits to the ΔE distributions using the full-MC line shape for the signal and a linear background. The background-subtracted data are then integrated between $\pm 2.0\sigma_{\Delta E}$. The correction for efficiency is obtained as described in Sec. V. A similar procedure is applied to the $\bar{B}^0 \to J/\psi K^-\pi^+$ and $B^+ \to J/\psi K^0_S\pi^+$ data.

The branching fraction for $\chi_{c1} \to J/\psi\gamma$ from Ref. [2] is 0.344 ± 0.015. Using this value, we obtain the following branching fraction ratios:

$$\frac{\mathcal{B}(\bar{B}^0 \to \chi_{c1}K^-\pi^+)}{\mathcal{B}(\bar{B}^0 \to J/\psi K^-\pi^+)} = 0.474 \pm 0.013 \pm 0.026 \quad (4)$$

and

$$\frac{\mathcal{B}(B^+ \to \chi_{c1} K^0 \pi^+)}{\mathcal{B}(B^+ \to J/\psi K^0 \pi^+)} = 0.501 \pm 0.024 \pm 0.028. \quad (5)$$

Systematic uncertainties are summarized in Table II and have been evaluated as follows:

(1) We obtain the uncertainty on the background subtraction by modifying the model used to fit the ΔE distributions. The signal was alternatively described by the sum of two Gaussian functions, and the background was parametrized by a second-order polynomial.
(2) We compute the uncertainty on the efficiency by making use of the binned efficiency on the $(m(K\pi), \cos\theta)$ plane. In each cell we randomize the generated and reconstructed yields according to Poisson distributions. Deviations from the fitted efficiencies give the uncertainty on this quantity.
(3) We vary the bin size for the binned efficiency calculation.
(4) We include a systematic error due to the uncertainty on the $\chi_{c1} \to J/\psi\gamma$ branching fraction [2].
(5) We assign a 1.8% uncertainty to the γ reconstruction efficiency.
(6) We modify the ΔE and $m_{\rm ES}$ selection criteria and assign systematic uncertainties based on the variation of the extracted branching fractions.

We note that the systematic uncertainties are dominated by the uncertainty on the $\chi_{c1} \to J/\psi\gamma$ branching fraction.

The branching fractions measured in Ref. [6] are

$$\mathcal{B}(\bar{B}^0 \to J/\psi K^- \pi^+) = (1.079 \pm 0.011) \times 10^{-3}, \quad (6)$$

$$\mathcal{B}(B^+ \to J/\psi K^0 \pi^+) = (1.101 \pm 0.021) \times 10^{-3}, \quad (7)$$

where the latter value has been corrected for K_L^0 and $K_S^0 \to \pi^0\pi^0$ decays [2].

Multiplying the ratio in Eq. (4) by the $\bar{B}^0 \to J/\psi K^- \pi^+$ branching fraction in Eq. (6), we obtain

$$\mathcal{B}(\bar{B}^0 \to \chi_{c1} K^- \pi^+) = (5.11 \pm 0.14 \pm 0.28) \times 10^{-4}. \quad (8)$$

TABLE II. Systematic uncertainties (%) for the $B \to \chi_{c1} K\pi$ relative branching fraction measurements.

Contribution	$\bar{B}^0 \to \chi_{c1} K^- \pi^+$	$B^+ \to \chi_{c1} K_S^0 \pi^+$
1. Background subtraction	1.6	1.0
2. Efficiency	1.5	1.6
3. Efficiency binning	1.1	1.9
4. χ_{c1} branching fraction	4.4	4.4
5. γ reconstruction	1.8	1.8
6. ΔE and $m_{\rm ES}$ selections	1.0	1.0
Total (%)	5.4	5.5

This may be compared to the Belle measurement [1]: $\mathcal{B}(\bar{B}^0 \to \chi_{c1} K^- \pi^+) = (3.83 \pm 0.10 \pm 0.39) \times 10^{-4}$.

Multiplying the ratio in Eq. (5) by the $B^+ \to J/\psi K^0 \pi^+$ branching fraction in Eq. (7), we obtain

$$\mathcal{B}(B^+ \to \chi_{c1} K^0 \pi^+) = (5.52 \pm 0.26 \pm 0.31) \times 10^{-4}, \quad (9)$$

so that, after all corrections, the branching fractions corresponding to decay modes (1) and (2) are the same within uncertainties.

VII. FITS TO THE $K\pi$ MASS SPECTRA

We perform binned-χ^2 fits to the background-subtracted and efficiency-corrected $K\pi$ mass spectra in terms of S, P, and D wave amplitudes. The fitting function is expressed as

$$\frac{dN}{dm} = N\left[f_S \frac{G_S(m)}{\int G_S(m)dm} + f_P \frac{G_P(m)}{\int G_P(m)dm} + f_D \frac{G_D(m)}{\int G_D(m)dm}\right], \quad (10)$$

where $m = m(K\pi)$, the integrals are over the full $m(K\pi)$ range, and the fractions f are such that

$$f_S + f_P + f_D = 1. \quad (11)$$

The P- and D-wave intensities, $G_P(m)$ and $G_D(m)$, are expressed in terms of the squared moduli of relativistic Breit-Wigner functions with parameters fixed to the PDG values for $K^*(892)$ and $K_2^*(1430)$, respectively [2]. For the S-wave contribution $G_S(m)$ we make use of the LASS [13] parametrization described by Eqs. (11)–(16) of Ref. [6].

The above model gives a good description of the data for the decays $B \to J/\psi K\pi$ [6]. However, for $B \to \chi_{c1} K\pi$ the above resonances do not describe the high mass region of the $K\pi$ mass spectra well. A better fit is obtained by including an additional incoherent spin-1 $K^*(1680)$ [2] resonance contribution. The fit results are shown by the solid curves in Fig. 7, and the resulting intensity contributions are summarized in Table III. In Figs. 7(a) and 7(b) the

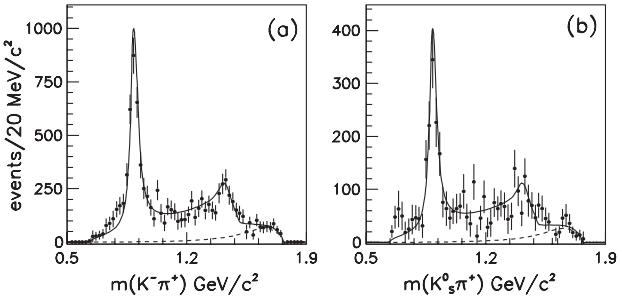

FIG. 7. Fits to the background-subtracted and efficiency-corrected $K\pi$ mass spectra for (a) $\bar{B}^0 \to \chi_{c1} K^- \pi^+$ and (b) $B^+ \to \chi_{c1} K_S^0 \pi^+$. The $K^*(1680)$ contribution is shown in each figure by the dashed curve.

TABLE III. S-, P-, D-wave fractions (in %), and χ^2/NDF (NDF = number of degrees of freedom) from the fits to the $K\pi$ mass spectra in $\bar{B}^0 \to \chi_{c1}K^-\pi^+$ and $B^+ \to \chi_{c1}K^0_S\pi^+$. The second P-wave entry in the two χ_{c1} channels corresponds to the fraction of $K^*(1680)$.

Channel	S wave	P wave	D wave	χ^2/NDF
$\bar{B}^0 \to \chi_{c1}K^-\pi^+$	40.4 ± 2.2	37.9 ± 1.3 10.3 ± 1.5	11.4 ± 2.0	58/54
$B^+ \to \chi_{c1}K^0_S\pi^+$	42.4 ± 3.5	37.1 ± 3.2 10.4 ± 2.5	10.1 ± 3.1	55/54

contributions due to the $K^*(1680)$ amplitude are shown by the dashed curves. The $\chi_{c1}K\pi$ decay modes differ from the corresponding $J/\psi K\pi$ and $\psi(2S)K\pi$ decay modes in that the S-wave fraction is much larger in the former than in the latter. This was observed for the $K^*(892)$ region in a previous *BABAR* analysis [14].

VIII. THE $K\pi$ LEGENDRE-POLYNOMIAL MOMENTS

We compute the efficiency-corrected Legendre-polynomial moments $\langle Y^0_L\rangle$ in each $K\pi$ mass interval by correcting for efficiency, as explained in Sec. V, and then weighting each event by the $Y^0_L(\cos\theta)$ functions. A similar procedure is performed for the ΔE sideband events, for which the distributions are subtracted from those in the signal region. We observe consistency between the $\bar{B}^0$ and B^+ data. Therefore, in the following we combine the $\bar{B}^0$ and B^+ distributions.

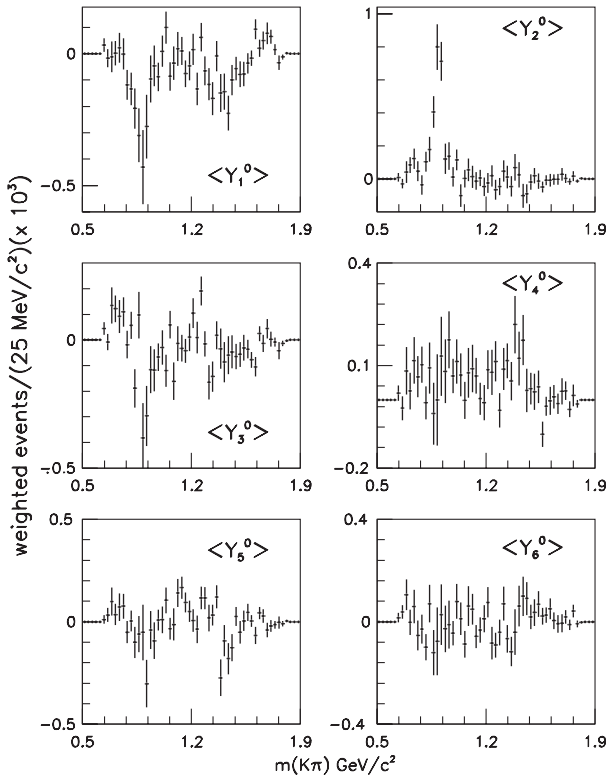

FIG. 8. Legendre-polynomial moments $\langle Y^0_L\rangle$ for $L = 1, \ldots, 6$ as functions of $K\pi$ mass for $B \to \chi_{c1}K\pi$ after background subtraction and efficiency correction.

This yields the background-subtracted and efficiency-corrected Legendre-polynomial moments $\langle Y^0_L\rangle$. They are shown for $L = 1, \ldots, 6$ in Fig. 8. We notice that the $\langle Y^0_6\rangle$ moment is consistent with zero, as are higher moments (not shown).

These moments can be expressed in terms of S-, P- and D-wave $K\pi$ amplitudes [15]. The P and D waves can be present in three helicity states and, after integration over the decay angles of the χ_{c1}, the relationship between the moments and the amplitudes is given by Eqs. (26)–(30) of Ref. [6]. We notice that, ignoring the presence of resonances in the exotic charmonium channel, the equations involve seven amplitude magnitudes and six relative phase values, and so they cannot be solved in each $m(K\pi)$ interval. For this reason, it is not possible to extract the amplitude moduli and relative phase values from Dalitz plot analyses of the $\psi K\pi$ or $\chi_{c1}K\pi$ final states.

In Fig. 8 we observe the presence of the spin-1 $K^*(890)$ in the $\langle Y^0_2\rangle$ moment and S-P interference in the $\langle Y^0_1\rangle$ moment. We also observe evidence for the spin-2 $K^*_2(1430)$ resonance in the $\langle Y^0_4\rangle$ moment. There are some similarities between the moments of Fig. 8 and those from $B \to J/\psi K\pi$ decays in Ref. [6]. However, we also observe a significant structure around 1.7 GeV/c^2 in $\langle Y^0_1\rangle$ which is absent in the $B \to J/\psi K\pi$ decays. We attribute this to the presence of the $K^*_1(1680)$ resonance produced in $B \to \chi_{c1}K\pi$ but absent in $B \to J/\psi K\pi$. The presence of scalar Z resonances should show up especially in high $\langle Y^0_L\rangle$ moments.

From the $\langle Y^0_L\rangle$ we obtain the normalized moments

$$\langle Y^N_L\rangle = \frac{\langle Y^0_L\rangle}{n}, \tag{12}$$

where n is the number of events in the given $m(K\pi)$ mass interval.

IX. MONTE CARLO SIMULATIONS

We model $B \to \chi_{c1}K\pi$ using the resonant structure obtained from the analysis of the $K\pi$ mass spectra and $K\pi$ Legendre-polynomial moments. For this purpose we

generate a large number of MC events according to the following procedure.

(i) $B \to \chi_{c1} K\pi$ events are generated uniformly in phase space [12]. The B mass is generated as a Gaussian line shape with parameters obtained from a fit to the data.

(ii) We weight each event by a factor $w_{m(K\pi)}$ derived from the resonant structure in the $K\pi$ system described in Sec. VII [Eq. (10)] and displayed in Table III.

(iii) We incorporate the measured $K\pi$ angular structure by giving weight w_L to each event according to the expression

$$w_L = \sum_{i=0}^{L_{\max}} \langle Y_i^N \rangle Y_i^0(\cos\theta). \tag{13}$$

The moments correspond to the combined data from the decay modes of Eqs. (1) and (2). The $\langle Y_i^N \rangle$ are evaluated for the $m(K\pi)$ value by linear interpolation between consecutive $m(K\pi)$ mass intervals.

(iv) The total weight is thus

$$w = w_{m(K\pi)} \cdot w_L. \tag{14}$$

The generated distributions, weighted by the total weight w, are then normalized to the number of data events obtained after background subtraction and efficiency correction.

We first test the method using as a control sample the combined data from $\bar{B}^0 \to J/\psi K^- \pi^+$ and $B^+ \to J/\psi K_S^0 \pi^+$, where no resonant structure is observed in the $J/\psi\pi$ mass distributions [6]. In this case we generate $B \to J/\psi K\pi$ events and use the $K\pi$ resonant structure and Legendre-polynomial information from the same channels. We compare the MC simulation to the $J/\psi\pi^+$ mass projection from data in Fig. 9. We obtain $\chi^2/\mathrm{NDF} = 223,\ 162,\ 180/152$ for $L_{\max} = 4,\ 5,\ 6$, respectively. We conclude that $L_{\max} = 5$ gives the best description of the data.

We now perform a similar MC simulation for $B \to \chi_{c1} K\pi$ using moments from the same channels. We obtain $\chi^2/\mathrm{NDF} = 53,\ 46,\ 49/58$ for $L_{\max} = 4,\ 5,\ 6$, respectively. The result of the simulation with $L_{\max} = 5$ is superimposed on the data in Fig. 10, and the corresponding χ^2/NDF is given in Table IV. The excellent description of the data indicates that the angular information from the $K\pi$ channel with $L_{\max} = 5$ is able to account for the structures observed in the $\chi_{c1}\pi$ projection. This indicates the absence of significant structure in the exotic $\chi_{c1}\pi^+$ channel.

We perform a MC simulation where, to the data from $\bar{B}^0 \to \chi_{c1} K^- \pi^+$, we add an arbitrary fraction ($\approx 25\%$) of events which include a $Z_2(4250)^+$ resonance decaying to $\chi_{c1}\pi$. These $Z_2(4250)^+$ events are obtained from phase-space MC $\bar{B}^0 \to \chi_{c1} K^- \pi^+$ events weighted by a simple Breit-Wigner function. We then compute Legendre-polynomial moments for the total sample and use them to predict the $\chi_{c1}\pi$ mass distribution as described above. The $\chi_{c1}\pi$ mass spectrum for these events is shown in Fig. 11(a). We obtain $\chi^2/\mathrm{NDF} = 103,\ 91,\ 88/58$ for $L_{\max} = 4,\ 5,\ 6$, respectively. Therefore, in the presence of a $Z_2(4250)^+$ resonance, it is not possible to obtain a good description of the $\chi_{c1}\pi$ mass distribution using $L_{\max} = 5$. We then increase the value of $L_{\max}$ and obtain a good description of this MC simulation with $L_{\max} = 15$, as

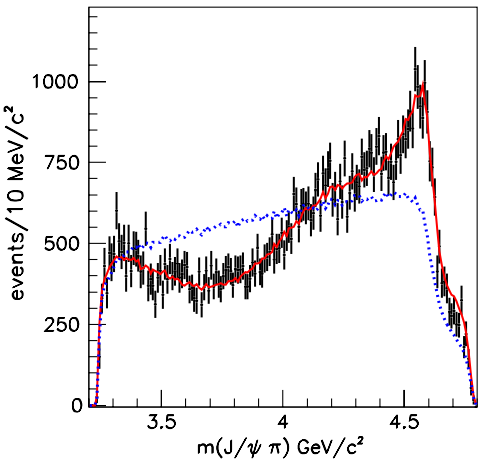

FIG. 9 (color online). Background-subtracted and efficiency-corrected $J/\psi\pi$ mass distribution for the $B \to J/\psi K\pi$ control sample with the superimposed curves resulting from the MC simulation described in the text. The solid curve is obtained using the total weight w obtained with $L_{\max} = 5$, and the dotted curve by omitting the angular-dependence factor w_L.

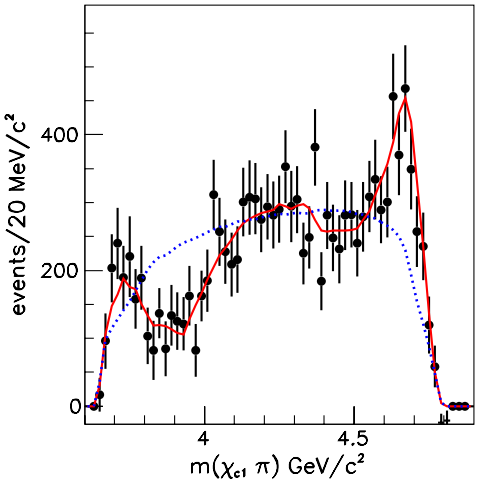

FIG. 10 (color online). Background-subtracted and efficiency-corrected $\chi_{c1}\pi$ mass distribution from $B \to \chi_{c1} K\pi$. The solid curve results from the MC simulation described in the text, which uses the moments from the same channels. The dotted curve shows the result of the simulation when the w_L weight is removed.

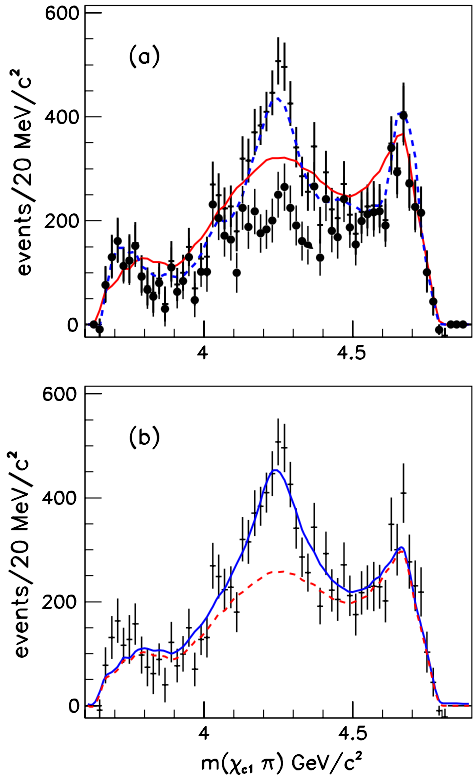

FIG. 11 (color online). Background-subtracted and efficiency-corrected $\chi_{c1}\pi$ mass distribution from $B \to \chi_{c1} K \pi$, which includes a simulated $Z_2(4250)^+$ (vertical crosses). In (a) the distribution with solid dots represents the $\bar{B}^0 \to \chi_{c1} K^- \pi^+$ data component. The continuous curve is the result from the mixed simulation described in the text and obtained from the MC simulation. The dashed curve shows a simulation with $L_{\max} = 15$. (b) Result from the fit described in the text, which incorporates a Breit-Wigner line shape describing the $Z_2(4250)^+$. The dashed curve represents the background model from the mixed simulation.

shown by the dashed curve in Fig. 11(a) ($\chi^2/\mathrm{NDF} = 57/58$).

We next test a "mixed" simulation where we use $L_{\max} = 3$ up to a $K\pi$ mass of 1.2 GeV/c^2 and $L_{\max} = 4$ for the rest of the events. This choice is justified by the presence of spin 0 and 1 resonances mostly in the low $K\pi$ mass region, while the $K_2^*(1430)$ contributes for $m(K\pi) > 1.2$ GeV/c^2. This simulation gives a satisfactory description of the $B \to \chi_{c1} K \pi$ data with $\chi^2/\mathrm{NDF} = 63/58$ but gives a bad description of the MC sample of Fig. 11(a), yielding $\chi^2/\mathrm{NDF} = 140/58$.

We now fit the MC sample including a simple Breit-Wigner function (with the width fixed to the simulated value) to describe the $Z_2(4250)^+$ [Fig. 11(b)]. We obtain the solid curve, which has $\chi^2/\mathrm{NDF} = 75/56$, a $Z_2(4250)^+$ mass consistent with the generated value, and a yield consistent with the generated one. The dashed curve represents the background model from the mixed simulation. The MC test therefore validates the use of this background model for a quantitative evaluation of the upper limits described in Sec. X.

The data-MC comparisons for the different simulations are summarized in Table IV.

X. SEARCH FOR $Z_1(4050)^+$ AND $Z_2(4250)^+$

We have shown, in the previous sections, that in the absence of Z resonances, the simulation with $L_{\max} = 5$ gives a good description of the $B \to J/\psi K \pi$ and $B \to \chi_{c1} K \pi$ data. We now test the possible presence of the $Z_1(4050)^+$ and $Z_2(4250)^+$ resonances in $B \to \chi_{c1} K \pi$ decay. Therefore, we adopt the minimum $L_{\max}$ configuration (mixed) described in Sec. IX and investigate whether something else is needed by the data.

For this purpose we perform binned χ^2 fits to the $\chi_{c1}\pi^+$ mass spectrum. In these fits the normalization of the background component is determined by the fit. We observe that this background model predicts an enhancement in the mass region of the Z resonances. We then add, for the signal, relativistic spin-0 Breit-Wigner functions with parameters fixed to the Belle values for the signals [1]. We compute statistical significance using the fitted fraction divided by its uncertainty.

We first perform fits to the total mass spectrum.

Fit (a) is shown in Fig. 12(a), and includes both $Z_1(4050)^+$ and $Z_2(4250)^+$ resonances.

Fit (b) is shown in Fig. 12(b), and includes a single broad $Z(4150)^+$ resonance.

In both cases the fits give fractional contributions consistent with zero for the Z resonances.

TABLE IV. The value of χ^2/NDF for different MC-data comparisons; "Y_L^N" indicates the channel used to obtain the normalized moments. The mixed algorithm is explained in the text. The definition of "window" is given in Sec. X.

Channel	Y_L^N	$L_{\max}$	χ^2/NDF
$B \to J/\psi K \pi$	$B \to J/\psi K \pi$	5	162/152
$B \to \chi_{c1} K \pi$	$B \to \chi_{c1} K \pi$	5	46/58
$B \to \chi_{c1} K \pi$	$B \to \chi_{c1} K \pi$	Mixed	63/58
$B \to \chi_{c1} K \pi$ window	$B \to \chi_{c1} K \pi$	5	45/47
$B \to \chi_{c1} K \pi$ window	$B \to \chi_{c1} K \pi$	Mixed	56/47

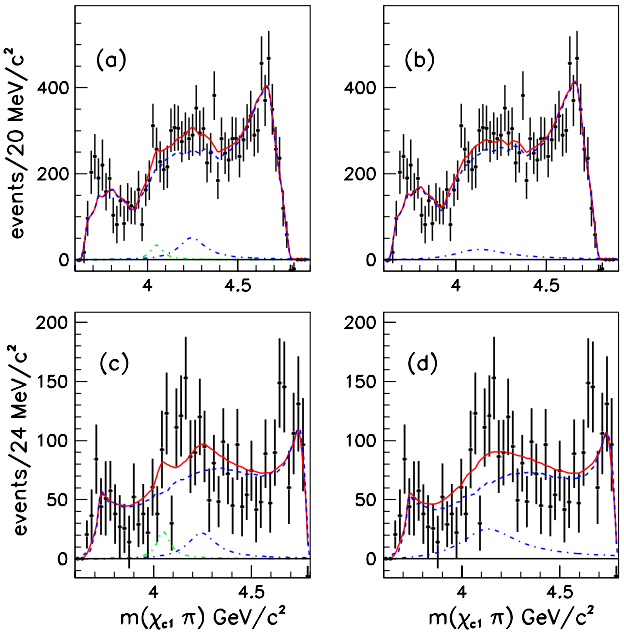

FIG. 12 (color online). (a), (b) Background-subtracted and efficiency-corrected $\chi_{c1}\pi$ mass distribution for $B \to \chi_{c1}K\pi$. (a) Fit with $Z_1(4050)^+$ and $Z_2(4250)^+$ resonances. (b) Fit with only the $Z(4150)^+$ resonance. (c), (d) Efficiency-corrected and background-subtracted $\chi_{c1}\pi$ mass distribution for $B \to \chi_{c1}K\pi$ in the $K\pi$ mass region $1.0 < m^2(K\pi) < 1.75$ GeV$^2/c^4$. (c) Fit with $Z_1(4050)^+$ and $Z_2(4250)^+$ resonances. (d) Fit with only the $Z(4150)^+$ resonance. In each fit the dashed curve shows the prediction from the mixed $B \to \chi_{c1}K\pi$ simulation explained in the text. The dot-dashed curves indicate the fitted resonant contributions.

We next fit the $\chi_{c1}\pi$ mass spectrum in the Dalitz plot region $1.0 \le m^2(K\pi) < 1.75$ GeV$^2/c^4$ in order to make a direct comparison to the Belle results [1]. Figures 12(c) and 12(d) show the $\chi_{c1}\pi$ mass spectrum for this mass region (labeled as "window" in Table V), where the Belle data show the maximum of the reported resonance activity. This sample accounts for 25% of our total data sample. Table IV gives the corresponding χ^2/NDF values for the MC simulations described in Sec. IX, in this mass window.

Fit (c) is shown in Fig. 12(c), and includes both $Z_1(4050)^+$ and $Z_2(4250)^+$ resonances.

Fit (d) is shown in Fig. 12(d), and includes a single broad $Z(4150)^+$ resonance.

In each case the fit gives a Z resonance contribution consistent with zero.

The results of the fits are summarized in Table V, and in every case the yield significance does not exceed 2σ. Similar results are obtained when the resonance parameters are varied within their statistical errors.

We compute upper limits integrating the region of positive branching fraction values for a Gaussian function having the above mean and σ values, and obtain the following 90% C.L. limits for the $Z_1(4050)^+$ and $Z_2(4250)^+$ resonances:

$$\mathcal{B}(\bar{B}^0 \to Z_1(4050)^+K^-) \times \mathcal{B}(Z_1(4050)^+ \to \chi_{c1}\pi^+) < 1.8 \times 10^{-5}, \quad (15)$$

$$\mathcal{B}(\bar{B}^0 \to Z_2(4250)^+K^-) \times \mathcal{B}(Z_2(4250)^+ \to \chi_{c1}\pi^+) < 4.0 \times 10^{-5}, \quad (16)$$

$$\mathcal{B}(\bar{B}^0 \to Z^+K^-) \times \mathcal{B}(Z^+ \to \chi_{c1}\pi^+) < 4.7 \times 10^{-5}. \quad (17)$$

Systematic uncertainties related to the Z parameters have been ignored since they give negligible contributions. The corresponding values for B^+ decay are $\approx 8\%$ larger [see Eqs. (8) and (9)].

Our measurements can be compared to the Belle results [1]:

$$\mathcal{B}(\bar{B}^0 \to Z_1(4050)^+K^-) \times \mathcal{B}(Z_1(4050)^+ \to \chi_{c1}\pi^+) = 3.0^{+1.5+3.7}_{-0.8-1.6} \times 10^{-5}, \quad (18)$$

$$\mathcal{B}(\bar{B}^0 \to Z_2(4250)^+K^-) \times \mathcal{B}(Z_2(4250)^+ \to \chi_{c1}\pi^+) = 4.0^{+2.3+19.7}_{-0.9-0.5} \times 10^{-5}. \quad (19)$$

Given the large uncertainties, these branching fraction values are compatible with our upper-limit estimates.

TABLE V. Results of the fits to the $\chi_{c1}\pi$ mass spectra. The columns N_σ and Fraction give, for each fit, the significance and the fractional contribution of the Z resonances.

Data	Resonance	N_σ	Fraction (%)	χ^2/NDF
a) Total	$Z_1(4050)^+$	1.1	1.6 ± 1.4	57/57
	$Z_2(4250)^+$	2.0	4.8 ± 2.4	
b) Total	$Z(4150)^+$	1.1	4.0 ± 3.8	61/58
c) Window	$Z_1(4050)^+$	1.2	3.5 ± 3.0	53/46
	$Z_2(4250)^+$	1.3	6.7 ± 5.1	
d) Window	$Z(4150)^+$	1.7	13.7 ± 8.0	53/47

XI. CONCLUSIONS

We use 429 fb^{-1} of data from the *BABAR* experiment at SLAC to search for the $Z_1(4050)^+$ and $Z_2(4250)^+$ states decaying to $\chi_{c1}\pi^+$ in the decays $\bar{B}^0 \to \chi_{c1}K^-\pi^+$ and $B^+ \to \chi_{c1}K^0_S\pi^+$, where $\chi_{c1} \to J/\psi\gamma$.

We measure the following branching fractions for the decays $\bar{B}^0 \to \chi_{c1}K^-\pi^+$ and $B^+ \to \chi_{c1}K^0\pi^+$:

$$\mathcal{B}(\bar{B}^0 \to \chi_{c1}K^-\pi^+) = (5.11 \pm 0.14 \pm 0.28) \times 10^{-4}$$

and

$$\mathcal{B}(B^+ \to \chi_{c1}K^0\pi^+) = (5.52 \pm 0.26 \pm 0.31) \times 10^{-4}.$$

In our search for the Z states, we first attempt to describe the data assuming that all resonant activity is concentrated in the $K\pi$ system. We use the decay $B \to J/\psi K\pi$ as a control sample, since no resonant structure has been observed in the $J/\psi\pi$ mass spectrum. In this case a good description of the data is obtained by a MC simulation which makes use of the known resonant structure in the $K\pi$ mass spectrum together with a Legendre-polynomial description of the angular structure as a function of $K\pi$ mass.

The same procedure is then applied to our data on the decays $B \to \chi_{c1}K\pi$, and a good description of the $\chi_{c1}\pi$ mass distribution is obtained. This indicates that no significant resonant structure is present in the $\chi_{c1}\pi$ mass spectrum, as observed for the $J/\psi\pi$ mass distribution [6]. We also observe that this background model predicts an enhancement in the mass region of the Z resonances. We then report 90% C.L. upper limits on possible $\bar{B}^0 \to Z^+K^-$ decays.

In conclusion, we find that it is possible to obtain a good description of our data without the need for additional resonances in the $\chi_{c1}\pi$ system.

ACKNOWLEDGMENTS

We are grateful for the extraordinary contributions of our PEP-II colleagues in achieving the excellent luminosity and machine conditions that have made this work possible. The success of this project also relies critically on the expertise and dedication of the computing organizations that support *BABAR*. The collaborating institutions wish to thank SLAC for its support and the kind hospitality extended to them. This work is supported by the US Department of Energy and National Science Foundation, the Natural Sciences and Engineering Research Council (Canada), the Commissariat à l'Energie Atomique and Institut National de Physique Nucléaire et de Physique des Particules (France), the Bundesministerium für Bildung und Forschung and Deutsche Forschungsgemeinschaft (Germany), the Istituto Nazionale di Fisica Nucleare (Italy), the Foundation for Fundamental Research on Matter (The Netherlands), the Research Council of Norway, the Ministry of Education and Science of the Russian Federation, Ministerio de Ciencia e Innovación (Spain), and the Science and Technology Facilities Council (United Kingdom). Individuals have received support from the Marie-Curie IEF program (European Union), the A. P. Sloan Foundation (USA), and the Binational Science Foundation (USA-Israel).

[1] R. Mizuk *et al.* (Belle Collaboration), Phys. Rev. D **78**, 072004 (2008).
[2] K. Nakamura *et al.* (Particle Data Group), J. Phys. G **37**, 075021 (2010), and partial update for the 2012 edition (http://pdg.lbl.gov).
[3] S. K. Choi *et al.* (Belle Collaboration), Phys. Rev. Lett. **100**, 142001 (2008).
[4] R. Mizuk *et al.* (Belle Collaboration), Phys. Rev. D **80**, 031104(R) (2009).
[5] N. Drenska *et al.*, Riv. Nuovo Cimento **033**, 633 (2010).
[6] B. Aubert *et al.* (BABAR Collaboration), Phys. Rev. D **79**, 112001 (2009).
[7] B. Aubert *et al.* (BABAR Collaboration), Nucl. Instrum. Methods Phys. Res., Sect. A **479**, 1 (2002).
[8] W. Menges, IEEE Nuc. Sci. Symp. Conf. Rec. **5**, 1470 (2006).
[9] The use of charge conjugate reactions is implied throughout this work.
[10] The J/ψ vertex position is used to define the three-momentum vector of the photon, and this is then added to the three-momentum of the associated e^+ or e^- at this vertex. The electron mass is then assigned to this modified three-momentum vector, and the resulting four-momentum vector is used in calculating $m(e^+e^-)$.
[11] H. Albrecht *et al.* (ARGUS Collaboration), Z. Phys. C **48**, 543 (1990).
[12] F. James, CERN Program Library, Report No. W515.
[13] D. Aston *et al.* (LASS Collaboration), Nucl. Phys. **B296**, 493 (1988); W. Dunwoodie (private communication).
[14] B. Aubert *et al.* (*BABAR* Collaboration), Phys. Rev. D **76**, 031102 (2007).
[15] S. T'Jampens, Ph.D. thesis, Université Paris XI, 2002; Report No. SLAC-R-836, Appendix D.